Influence of Additives on the Reversible Oxygen Reduction Reaction/Oxygen Evolution Reaction in the Mg^{2+}-Containing Ionic Liquid *N*-Butyl-*N*-Methylpyrrolidinium Bis(Trifluoromethanesulfonyl)imide

M. Eckardt[+],[a, b, c] D. Alwast[+],[a, b, c] J. Schnaidt,[a] and R. J. Behm*[a, b]

The influence of different additives on the oxygen reduction reaction/oxygen evolution reaction (ORR/OER) in magnesium-containing *N*-butyl-*N*-methylpyrrolidinium bis(trifluoromethanesulfonyl)imide ([BMP][TFSI]) on a glassy carbon electrode was investigated to gain a better understanding of the electrochemical processes in Mg–air batteries. 18-Crown-6 was used as a complexing agent for Mg ions to hinder the passivation caused by their reaction with ORR products such as superoxide and peroxide anions. Furthermore, borane dimethylamine complex (NBH) was used as a potential water-removing agent to inhibit electrode passivation by reacting with trace impurities of water. The electrochemical processes were characterized by differential electrochemical mass spectrometry to monitor the consumed and evolved O_2 in the ORR/OER and determine the number of transferred electrons. Crown ether and NBH efficiently masked Mg^{2+}. A stochiometric excess of crown ether resulted in reduced formation of a passivation layer, whereas at too high concentrations the reversibility of the ORR/OER was diminished.

Introduction

The physical limitations of Li-ion battery systems have motivated the search and development of new batteries with potentially higher energy densities and based on more abundant materials. Most prominent, secondary metal–air batteries are seen as the next step for increasing energy density, ecology, and economy of energy storage compared with Li-ion batteries.[1,2–11] Using air-based cathodes can increase the theoretical energy density by replacing the commonly used cathode materials that contain large amounts of, for example, cobalt and nickel, with lighter materials. Here, the oxygen is provided by the ambient air while discharging, during which it is reduced to superoxide or peroxide species in the oxygen reduction reaction (ORR) and released again during charging by the oxygen evolution reaction (OER).[1,9–11]

Promising next generation battery systems are secondary Mg–air batteries in which the lithium is replaced by magnesium, which is not only more abundant than lithium but also has advantages regarding safety aspects.[12–14] Additionally, the volumetric capacity of magnesium exceeds that of lithium by almost a factor of two.[12] However, the slow reaction kinetics of magnesium intercalation/insertion in the Mg–air battery reactions are largely caused by the slow diffusion of Mg in the anode.[13] Furthermore, the formation of stable magnesium oxides in the presence of water strongly limits the reversibility of Mg–air batteries.[14] This "breathing" and therefore open battery system causes specific demands for the electrolyte, which should neither evaporate from the battery nor be sensitive to air. Furthermore, the stability of the electrolyte towards reduction products that are formed during the ORR is a key factor.[15–17]

Ionic liquids (ILs) seem to be a good choice as electrolytes as they provide the required stability and a low vapor pressure.[18–22] However, applying ILs as electrolytes for Mg–air batteries (IL containing Mg^{2+}) has been shown to result in a slow deposition/dissolution of Mg on the anode and a strong passivation on the cathode, whereby the latter results in a strongly limited ORR/OER reversibility.[23–28] Furthermore, on the anode side, strong interactions between Mg^{2+} and bis(trifluoromethanesulfonyl)imide ($TFSI^-$) were speculated to cause a high overpotential for Mg deposition, resulting in the decomposition of the electrolyte, which in turn leads to the formation of a passivating film on the anode.[23,29] It is well known from pre-

[a] Dr. M. Eckardt,[+] D. Alwast,[+] Dr. J. Schnaidt, Prof. R. J. Behm
Institute of Surface Chemistry and Catalysis
Ulm University
Albert-Einstein-Allee 47, 89081 Ulm (Germany)
E-mail: juergen.behm@uni-ulm.de

[b] Dr. M. Eckardt,[+] D. Alwast,[+] Prof. R. J. Behm
Helmholtz Institute Ulm (HIU) Electrochemical Energy Storage
Helmholtzstr. 11, 89081 Ulm (Germany)

[c] Dr. M. Eckardt,[+] D. Alwast[+]
Karlsruhe Institute of Technology (KIT)
P.O. Box 3640, 76021 Karlsruhe (Germany)

[+] These authors contributed equally to this work

Supporting Information and the ORCID identification number(s) for the author(s) of this article can be found under: https://doi.org/10.1002/cssc.202000672.

vious studies that the Mg plating and stripping characteristics can be improved by the use of additives.[30–32] However, their influence on the cathode reactions (ORR/OER) is largely unknown. For Li-air batteries, the addition of barium ions to the Li^+-containing electrolyte was reported to show promising effects on the discharge capacity, which was attributed to the incorporation of Ba^{2+} in the Li_2O_2 lattice.[33] For Mg–air batteries, we are not aware of any data on the influence of additives on the cathode reactions in aprotic electrolytes. In the present study, we investigated the influence of additives on the cathode reactions in Mg^{2+}-containing electrolytes, more specifically, on their impact on the passivation of the electrode and the ORR/OER reversibility.

We characterized the influence of the complexing agent 18-crown-6 and the water-removing additive borane dimethylamine complex (NBH) on the ORR/OER in 0.1 M $Mg(TFSI)_2$-containing *N*-butyl-*N*-methylpyrrolidinium bis(trifluoromethanesulfonyl)imide ([BMP][TFSI]) on a glassy carbon (GC) electrode. The measurements were performed in an electrochemical flow cell, employing online mass spectrometry analysis (differential electrochemical mass spectrometry (DEMS))[25,28,34] of the O_2 content of the electrolyte. This allowed us to determine the amount of O_2 consumed and evolved in the ORR and the OER, respectively, and calculate the number of electrons transferred per O_2 molecule in the reaction, which provides detailed insights into the processes on the electrode.[25,28,34]

The solubility of $Mg(TFSI)_2$ in THF-based electrolytes has been improved with the addition of 18-crown-6, which also leads to an increase in the ion conductivity.[35] Using the IL *N*-methyl-*N*-propylpiperidinium–TFSI ([PMP][TFSI]), a promoting effect on the Mg plating was reported by Sagane et al. for a $Mg(TFSI)_2$/[PMP][TFSI] = 1:5 mol electrolyte.[32] However, little is known about the influence of 18-crown-6 on the ORR/OER reversibility and the passivation of the cathode surface. Complexing Mg^{2+} on the cathode side might help "masking" of the magnesium ions for the ORR, mimicking a Mg^{2+}-free electrolyte and, thus, hindering or even suppressing the formation of a passivation layer. This would allow a reversible ORR/OER, as observed in neat [BMP][TFSI].[25,28,34,36] In that electrolyte, the ORR proceeds in two reaction steps, forming superoxide first, followed by the formation of peroxide at lower potentials.

Considering the effects of trace impurities of water, residual water in the electrolyte was shown to have a promoting effect on ORR in aprotic electrolyte.[34,37–39] It also enhances the formation of non-oxidizable magnesium peroxides and oxides in Mg^{2+}-containing electrolyte in the ORR, thus passivating the electrode.[14] Therefore, we also explored the effect of boron hydride as a water removing additive in the electrolyte. Boron hydride is known to react with water, forming H_2 and borate, and this way efficiently removes traces of water.

In the following, we start with a short description of the influence of $Mg(TFSI)_2$ on the ORR/OER in [BMP][TFSI], which will be used as a reference for the following systems (first section). Next, we present and discuss the results obtained on the influence of the 18-crown-6 complexing agent (second section) and the water-removing NBH additive (third section). In the next section, we summarize the most important findings obtained in this work. Finally, a brief description of the experimental set-up and the electrolytes used is presented.

Results and Discussion

Influence of $Mg(TFSI)_2$ on the ORR in [BMP][TFSI]

The addition of magnesium in the form of $Mg(TFSI)_2$ to [BMP][TFSI] introduces significant changes in the ORR/OER behavior on GC electrodes, as shown earlier by our group.[25–28] This is illustrated in Figure 1, which shows results of a potentiodynamic DEMS measurement performed in a potential window of −1.4 to 1.4 V versus Mg/MgO in neat [BMP][TFSI] (a–c) and in 0.1 M $Mg(TFSI)_2$ containing [BMP][TFSI] (d–f). Both times we show the 1st and the 4th cycle. In the cyclic voltammogram (CV) (Figure 1 a,d) we find distinct ORR currents starting at potentials below 0.4 and 0.7 V, respectively. In the positive-going scan, low faradaic current densities starting at approximately 0.4 V were observed. However, the charge transferred in the OER was much lower than that transferred in the ORR. This was mainly caused by the experimental conditions, because in the flow cell setup the products of the ORR are transported away from the electrode and, thus, cannot be oxidized again in the

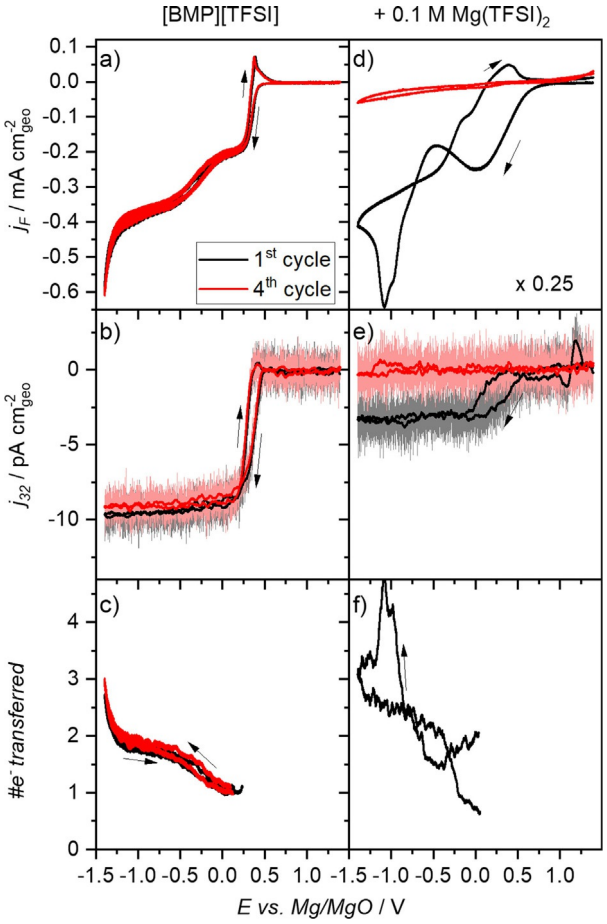

Figure 1. ORR/OER on glassy carbon in O_2-saturated (a–c) neat [BMP][TFSI] and (d–f) 0.1 M $MgTFSI_2$-containing [BMP][TFSI] at a scan rate of 10 mV s^{-1}. The first and fourth cycles are shown.

OER.[25] Therefore, this setup is not well suited to reproduce the ORR/OER reversibility in real battery systems, in which the ORR products can diffuse back to the electrode surface for further oxidation in the absence of any electrolyte flow. In the present experiments, it was not possible to detect the O_2 evolution by mass spectrometry owing to the low amounts of O_2 formed in both pure and $Mg(TFSI)_2$-containing [BMP][TFSI]. This is in contrast to results in our previous study,[25] in which we used a lower flow rate. As already discussed earlier,[25,,27,28,34] two plateaus were observed in the measured ORR signal in pure [BMP][TFSI], whereas the consumption of O_2 does not change in the measured potential window of the ORR (see Figure 1b). The first plateau appeared between 0.25 and 0 V, which we assumed to correspond to a one-electron transfer, as shown in Figure 1c. Therefore, in this potential range superoxide is formed during O_2 reduction.[36,40,41] Between −0.6 and −1.2 V a second plateau appeared with approximately twice the current density, which corresponds to a two-electron transfer and thus related to the formation of a peroxide.[25,34,42] Decreasing the potential further resulted in an increase in the current density with unchanged oxygen consumption. Therefore, we attribute the current increase to side reactions such as the decomposition of the IL or reduction of residual water impurities in the electrolyte.[25,29,34]

Comparing the ORR in pure [BMP][TFSI] with the ORR in $Mg(TFSI)_2$-containing IL, a much lower ORR current density was observed in the first cycle. However, there seemed to be two current plateaus, one between 0 and −0.5 V and the other appears to start at −0.9 V. However, in this case the current quickly decayed at more negative potentials. The oxygen consumption stayed approximately constant in the ORR potential window. In the presence of $Mg(TFSI)_2$, the number of electrons transferred was approximately 1.5 in the potential region of the first plateau, indicating that the product at least partly consisted of superoxides. We cannot specify whether the additional electrons come from partial formation of peroxides or other side reactions with the electrolyte. In the lower potential range below −0.5 V the electron transfer rapidly increased up to $>4e^-$ per O_2 molecule. The side reactions clearly played a role and seem to result in a passivation of the electrode surface. These results agree with findings in previous studies, which have reported that magnesium superoxide and magnesium peroxide are formed in this electrolyte, with the latter being the dominant product under most reaction conditions.[25–28] Even though a quantitative comparison of the current densities was not possible because of the differences in the O_2 content in the electrolyte in different measurements, the current densities in the $Mg(TFSI)_2$-containing electrolyte were much smaller than in the Mg-free electrolyte. In both electrolytes, in the presence and absence of $Mg(TFSI)_2$, superoxide species were formed at lower overpotentials in the ORR whereas at more negative potentials more electrons were transferred, indicating peroxide formation. After 4 cycles, the ORR was barely visible in the CV in Figure 1d, and the *m/z* 32 signal for O_2 does not show any oxygen consumption in the fourth cycle. Apparently, the ORR was inhibited by the formation of an ORR- and OER-inactive passivation layer on the electrode. This passivation of the electrode is a major drawback of this IL electrolyte for Mg–air batteries. Interestingly, passivation seems to be less of a problem in other aprotic electrolytes such as perchlorate in DMSO[45] and in Mg^{2+}-containing THF, in which peroxide is predominantly formed upon reduction, presumably by an electrochemical one-electron reduction to superoxide, followed by a chemical reduction step to peroxide.[46–48]

ORR/OER in the presence of crown ether additive

Additives such as crown ethers can help mask the magnesium by complexation and possibly suppress or even inhibit the formation of a passivation layer. ORR/OER measurements in electrolytes containing 18-crown-6 as complexing agent are presented in Figure 2. The ORR/OER in a 1:1 $Mg(TFSI)_2$/18-crown-6 electrolyte is shown in Figure 2a. Theoretically, this should result in full complexation of Mg^{2+}, provided every Mg^{2+} ion is complexed by one crown ether molecule, for 0.1 M 18-crown-6 and 0.1 M $Mg(TFSI)_2$.[35] In contrast to an improved ORR/OER performance and reversibility we expected, we obtained a faster passivation, with the electrode being fully passivated in the second cycle. Additionally, we obtained a peak at approximately −0.2 V in the first cycle, which is correlated with O_2 consumption and corresponds to the ORR. Such a peak was not observed in the 0.1 M $Mg(TFSI)_2$ electrolyte without addition of crown ether. In this peak the number of transferred electrons was approximately 1, in agreement with superoxide formation (Figure 2c). At more negative potentials, below approximately −0.5 V, the current passes through a minimum and then increases slowly up to the negative potential limit. In this range the number of electrons transferred per O_2 slowly increased to approximately 2. This is compatible with a slow transition from superoxide formation to peroxide formation, although reductive side reactions are also likely, causing the extended passivation of the electrode surface in this electrolyte. Different from the case of additive-free electrolyte, there is no indication of an OER signal in the positive-going scan (Figure 2a), indicating the formation of a stable passivation layer. Clearly, stoichiometric amounts of 18-crown-6 accelerate the passivation of the glassy carbon electrode instead of lowering it.

The effect of the crown ether changed if its concentration was increased to a $MgTFSI_2$/18-crown-6 ratio of 1:2 (Figure 2d). Most noticeable is the high current density in the first cycle, which exceeds that obtained in the crown ether free 0.1 M $MgTFSI_2$ electrolyte (see Figure 1) by more than a factor of 5. This is likely to be related to an efficient complexing and masking of the Mg ions, resulting in a less efficient passivation, at least in the first cycle. This high current density in the first cycle is followed by a pronounced decay below −0.7 V. In the second cycle, the current densities are small compared with the first cycle, but they do not change much after the second cycle up to the fourth cycle. The number of transferred electrons in the negative-going scan of the first cycle is between 3 and 4, indicating preferential formation of (su)peroxide plus some contributions either from magnesium oxide formation or other side reactions. In the subsequent cycles, the transfer of

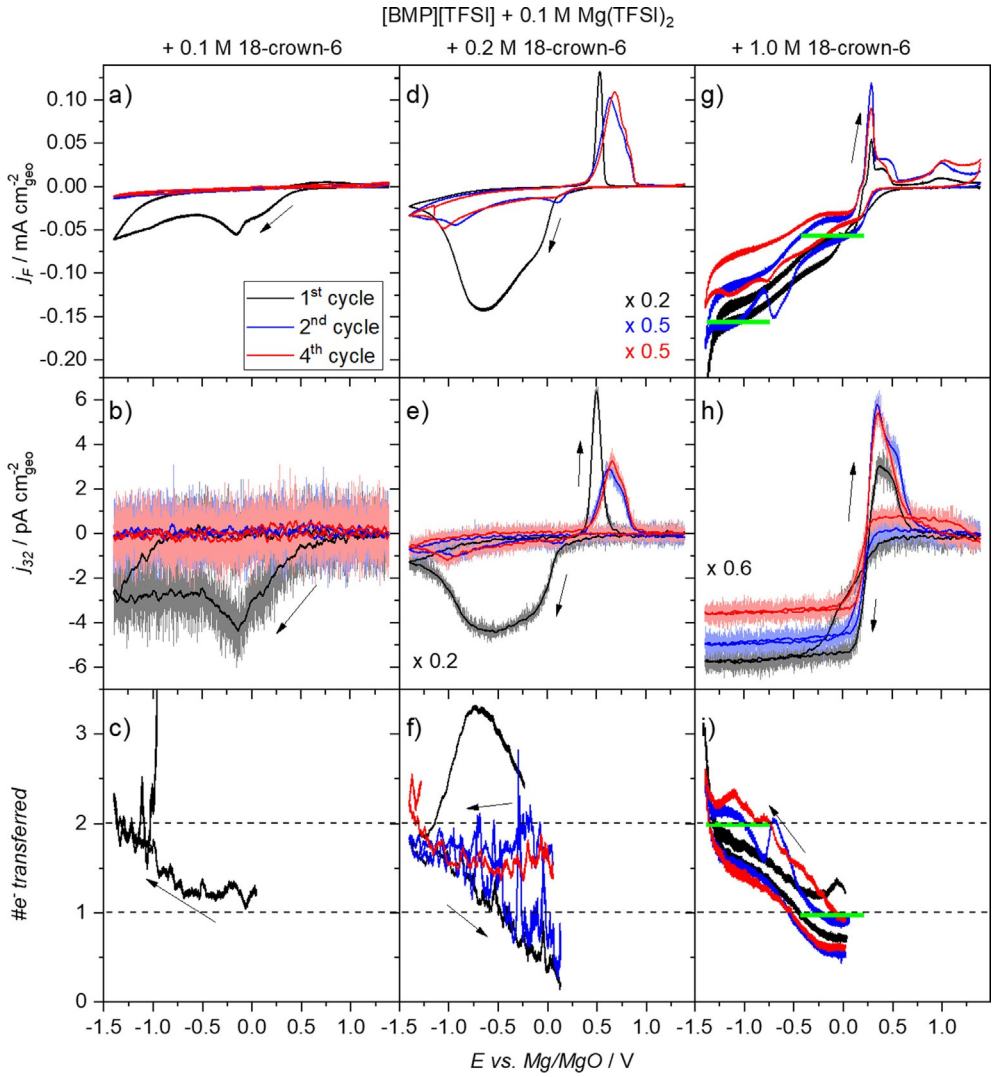

Figure 2. ORR/OER on glassy carbon in O_2-containing [BMP][TFSI] with 0.1 M $Mg(TFSI)_2$ and (a–c) 0.1 M, (d–f) 0.2 M, and (g–i) 1.0 M 18-crown-6 complexing additive at a scan rate of 10 mV s^{-1}.

only approximately 2 electrons per O_2 molecules in the negative-going scan points to the formation of peroxides (Figure 2 f). The observation of peroxide formation without continuing passivation could be a consequence of Mg^{2+} complexation, hindering the formation of solid magnesium peroxide deposits, although peroxide anions are formed continuously. Clearly, at these high concentrations, the crown ether can efficiently complex the Mg ions, which are no longer directly coordinated to peroxide ions. Therefore, mainly peroxides without direct coordination to Mg^{2+} ions are formed, as it was the case in pure [BMP][TFSI], which do not passivate the electrode surface. Considering the number of transferred electrons of up to 3 in the potential region 0 to −0.7 V, the strong passivation in the first negative-going scan at potentials < -0.7 V, which is evident both from the Faradaic current and from the mass spectrometric O_2 signal, can be tentatively explained by the formation of magnesium oxide. Presumably, the formation of magnesium oxide is not suppressed by the crown ether because of a stronger binding of O^{2-} to Mg^{2+}, and hence a lower solubility product as compared with binding to the crown ether, whereas for MgO_2 formation this seems to be opposite.

The reversibility of the ORR/OER benefits greatly from the addition of higher concentrations of the crown ether. In the positive-going scan of the first cycle, the OER appears as a sharp peak at 0.5 V, which is getting broader and shifts to about 0.7 V in the next cycle where it remains in the following cycles. Our interpretation is confirmed by the mass spectrometric data, which show a clear *m/z* 32 signal in parallel to these peaks (Figure 2 e). Interestingly, the total charge in the OER related peaks is almost constant in the different cycles, indicating that the absolute amount of re-oxidizable ORR products remains constant.

The presence of the OER signal points to the formation of a partly oxidizable layer on the electrode after the reductive scan. This can be explained by the formation of oxidizable peroxide species in the ORR rather than the formation of the passivating magnesium peroxide species. Integration of the Faradaic ORR and OER current signals in the second and fourth

cycle show a ratio of approximately 2:1 (ORR/OER). Therefore, despite the electrolyte flow, approximately half of the reduced oxygen species is essentially deposited on the electrode in this layer. The remaining part is either transported away with the flowing electrolyte or it is present in an inert, nonoxidizable state. Because the passivation stops after the first cycle, we favor the former explanation, at least after the first cycle. In the OER peak, the number of transferred electrons is about 1.3, which is a comparable order of magnitude as the number of electrons transferred per O_2 in the ORR (>1). The reversibility of the ORR/OER process indicates that there are indeed contributions from reversible peroxide formation and re-oxidation in the ORR/OER.

The addition of stoichiometric excess of 18-crown-6 to the electrolyte improves the ORR/OER characteristics. Therefore, we further increased the relative amount of the crown ether to a $MgTFSI_2$/18-crown-6 ratio of 1:10, which again resulted in significant changes in the ORR/OER (Figure 2g). The main difference is the absence of the passivation peak in the first cycle. The current densities in the second cycle are similar to those in the first cycle, and they are of similar order of magnitude as in the first cycle in the crown-ether-free electrolyte. The resulting CV closely resembles that obtained in pure [BMP][TFSI], showing also a two-plateau system (green bars in Figure 2g), a largely reduced passivation, and a clear OER signal. For the first plateau, the calculated number of electrons is approximately one. This number steadily increases with decreasing potential, reaching a value of approximately 2 in the range of the second plateau. In contrast to the measurements of the samples with lower amounts of crown ether in the electrolyte, the two-plateau structure is also remained in the subsequent cycles. Therefore, the presence of a high stoichiometric excess of crown ether in the electrolyte leads to a similar ORR behavior as in neat [BMP][TFSI]. In both electrolytes, there is an increase in the electron transfer per O_2 with increasing overpotential in the ORR, which, in contrast to the electrolytes with no or lower concentrations of crown ether, persists after multiple cycles. Therefore, we expected that the same transition from superoxide to peroxide formation observed for the ORR in neat [BMP][TFSI] occurs in 1:10 $MgTFSI_2$/18-crown-6-containing electrolyte when scanning to more negative potentials. In contrast to the situation in 0.2 M 18-crown-6, we did not detect the formation of magnesium oxide (electron number above 2). Under these conditions, Mg^{2+} complexation appears to be sufficiently efficient to fully inhibit MgO formation. Similar to the reaction in neat [BMP][TFSI], only peroxide and superoxide are formed, without formation of a passivating layer. In the second cycle, a distinct peak is observed at approximately -0.7 V in the negative-going scan, which was not present in the mass spectrometry O_2 signal (Figure 2g,h). Therefore, it is most probably not part of the O_2 reduction itself. This peak vanishes after further cycling. Therefore, we attribute the peak to the reduction of impurities in the crown ether.

A strong discrepancy between the integrated charges was observed at a ratio of approximately 10:1 (ORR/OER). This is much larger than the ratio of 2:1 that we obtained for the electrolyte with 0.2 M crown ether, but lower than for neat [BMP][TFSI] (300:1). We attribute the distinct difference between the two electrolytes, 0.1 M $Mg(TFSI)_2$ in [BMP][TFSI] and 1.0 M crown-ether-containing 0.1 M $Mg(TFSI)_2$ in [BMP][TFSI], to the strongly suppressed formation of a surface layer containing Mg-superoxide, peroxide, and oxide, to the efficient complexation of the Mg^{2+}. This allows the ORR products to be flushed away more easily, thus, decreasing the amount of oxidized ORR products in the OER. Therefore, a high stoichiometric excess of crown ether is helpful for decreasing the passivation but also reduces the reversibility of the OER in the flow-cell. The latter aspect does not apply in the case of battery applications, in which electrolyte flow is absent and the ORR products can reach the electrode surface by diffusion. Positive effects of the addition of crown ether to IL-based electrolytes with TFSI anions were also reported for Mg plating and stripping.[32,43] In that case, both plating and stripping are enhanced and the tendency for passivation is lowered, equivalent to an improved reversibility. This was explained by the (partial) displacement of TFSI anions from the Mg^{2+} coordination shell by the (stronger interacting) crown ether. This inhibits the formation of Mg^{2+}–$TFSI^-$ species, which were proposed to lead to TFSI decomposition upon electron transfer to the Mg^{2+} ion.[44] For the ORR, the stronger interaction between crown ether and Mg^{2+} is also favorable, as it reduces the formation of stable Mg^{2+} (su-)peroxide species. Finally, the calculated number of transferred electrons in the OER is approximately one, indicating that superoxide species are oxidized to O_2.

For further information on the influence of the crown ether on the electrolyte layer, we recorded SEM images of the surface obtained after 10 cycles ORR/OER in the absence and presence (1.0 M 18-crown-6) of crown ether (Figure 3). In the low-magnification images (Figure 3a), a distinct highly structured surface morphology is obtained when a 18-crown-6-free 0.1 M $Mg(TFSI)_2$ electrolyte was used, which is different from that of the GC substrate and, therefore, associated with a layer of magnesium oxide species on top of the GC. This is consistent also with the observation of Mg and O signals in EDX images (see the Supporting Information). Higher magnification reveals the formation of lengthy, rod-like structures (Figure 3b). Similar structures were reported by Bozorgchenani et al.[26] for 0.1 M $Mg(TFSI)_2$ in [BMP][TFSI] on a Pt surface. Adding the crown ether (1.0 M) resulted in different structures (Figure 3c). At higher magnification, a surface layer is observed, which seems to be thinner than the one obtained with the former electrolyte. This correlates well with the lower tendency for passivation and the increasing ORR/OER reversibility, supporting our previous claim that masking the Mg ions with crown ether reduces the amount of MgO_x in the surface layer and thus its passivating properties. Nevertheless, EDX measurements revealed the presence of oxidic magnesium species on these surfaces (Figure 3d), but significantly less than in the crown-ether-free electrolyte (Figure S1, Supporting Information).

Overall, the addition of crown ether in excess concentrations strongly influences the ORR/OER behavior in $Mg(TFSI)_2$-containing [BMP][TFSI]. The most important positive effect is the decreasing tendency for passivation as compared with only

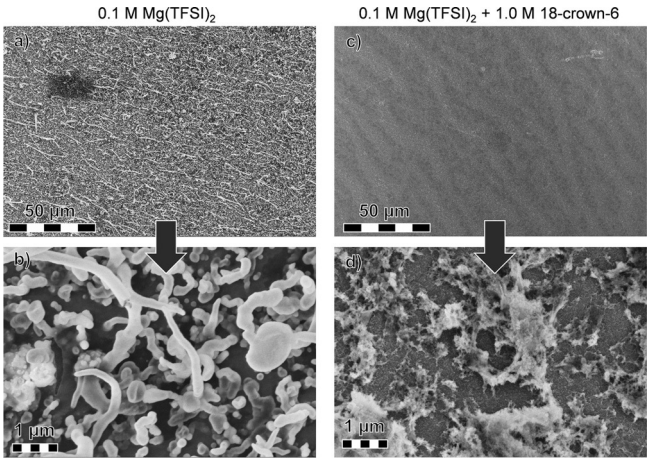

Figure 3. SEM images of the electrode surface recorded after 10 ORR cycles (−1.4–1.4 V; 10 mV s^{-1}) in (a,b) 0.1 M $Mg/TFSI)_2$ and in (c,d) 0.1 M $Mg(TFSI)_2$ and 1.0 M 18-crown-6 in [BMP][TFSI] (4.00 kV).

$Mg(TFSI)_2$-containing IL. The passivation process is slowed down considerably when crown ether is added in a tenfold excess to $Mg(TFSI)_2$. On the other hand, although high concentrations of crown ether are beneficial for suppressing the passivation, too high amounts (1.0 M) also lower the formation of oxidizable species such as Mg superoxides at or close to the electrode surface, which reduces the reversibility of the ORR and OER.

Drying agents

A major factor that contributes to the passivation of an electrode is residual water in the electrolyte; traces of water in magnesium-containing electrolytes are known to promote the formation of a nonoxidizable, passivating electrode layer in the ORR, consisting of magnesium oxide and peroxide.[14] Therefore, for the experiments presented in the previous sections, the electrolyte was dried before use in a UHV chamber to decrease the water content. Efficient ways to keep the electrolyte dry are needed, especially for metal-air batteries, in which the electrolyte is in contact with air. In these cases, self-drying electrolytes are highly desirable. Such effects can be achieved by the addition of drying agents such as borohydrides to the electrolyte. We explored the effect of adding such a drying agent on the reversibility of the ORR/OER and on the electrode passivation. In the first step, we added 0.01 M NBH to the $Mg(TFSI)_2$-containing [BMP][TFSI]. In these cases, the electrolyte was used as-is, without prior drying in vacuum. The CVs recorded in NBH-free and in NBH-containing electrolyte are presented in Figure 4. Karl Fischer titration demonstrated that the addition of NBH reduced the water content of (non-dried) [BMP][TFSI] to 20 ppm, as compared with $Mg(TFSI)_2$-containing [BMP][TFSI] (25 ppm) and 0.1 M 18-crown-6 + 0.1 M $Mg(TFSI)_2$-containing [BMP][TFSI] ((35 ppm). The CVs in Figure 4 clearly illustrate the strong influence of the addition of NBH in the first cycle in the ORR (Figure 4 a,d). The removal of water results in a significant increase of the ORR and OER current densities in the first cycle as compared with 0.1 M $Mg(TFSI)_2$ in [BMP][TFSI] electrolyte

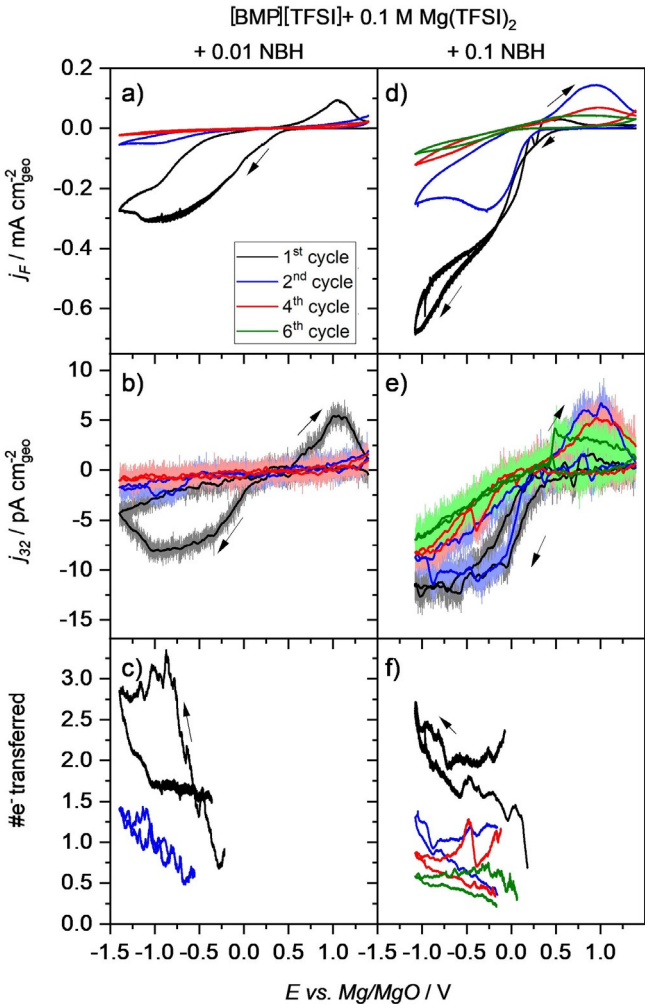

Figure 4. ORR/OER on a glassy carbon electrode in O_2-containing [BMP][TFSI] with 0.1 M $Mg(TFSI)_2$ and the NBH additive: (a,b,c) 0.01 M NBH and (d,e,f) 0.1 M NBH at a scan rate of 10 mV s^{-1}.

(see first section). However, for addition of 0.01 M NBH already the second cycle shows a similar extent of passivation as obtained in NBH-free electrolyte (Figure 1 d). Furthermore, in the first cycle the ORR also shows a rather high number of transferred electrons of approximately 2 and above, whereas in the second cycle this decreases to approximately one transferred electron per O_2 molecule. This indicates the formation of magnesium peroxide, causing the strong passivation during the first cycle, but not to the same degree as the NBH-free electrolyte (see Figure 1 d). The high current density in the first cycle could be owed to interactions between the $Mg(TFSI)_2$ and the NBH, which could lead to complexation of Mg^{2+}, similar to the behavior of crown ether discussed in the previous section. Interestingly, in the subsequent OER, there is only one electron transferred per O_2, which is consistent with a mechanism in which only the superoxide species can be re-oxidized. O_2 formation was not be observed for the oxidation of peroxide species to superoxides.

Increasing the concentration of NBH (Figure 4 d,e,f) results in even higher current densities of the ORR, but not for the OER,

in the first cycle. The first cycle is also dominated by the formation of peroxide (two-electron transfer), whereas in the subsequent cycles a one electron transfer to superoxide prevails. For this electrolyte, the lower potential limit was set to −1.1 instead of −1.4 V in the previous experiments (Figures 1–3) to not exceed the current density limitation of the flow cell. Significantly lower current densities are observed in the second cycle compared with the first cycle, indicative of surface passivation. Even though strong passivation is also observed for the 0.1 M NBH-containing electrolyte, the overall rate of passivation is decreased significantly. This is illustrated by the measurable ORR currents even in the sixth cycle of the 0.1 M NBH-containing electrolyte (Figure 4d), in contrast to the essentially complete passivation in the 0.01 M NBH-containing electrolyte (Figure 4a). Furthermore, there is also an improved ORR/OER reversibility compared with the 0.01 M NBH-containing electrolyte, with a more pronounced OER peak at approximately 1.0 V, which appears in the second cycle, in contrast to the 0.01 M NBH electrolyte, for which the peak only appears in the first cycle. The measurable OER peak in the latter case is most likely related to the fact that also the ORR signal is much higher in the second cycle than in the 0.01 M NBH-containing electrolyte.

Integration of the ORR and the OER signals reveals an increase in the reversibility of these reactions with increasing cycle number, as indicated by their current densities, with a ratio of the ORR/OER charge of 3:1 in the second cycle, which changes to 1.7:1 in the sixth cycle. This is in agreement with a change in the number of transferred electrons in the OER from 1.4 in the second cycle to approximately 1 in the sixth cycle. This ORR/OER charge ratio is similar to that obtained for the 0.2 M 18-crown-6 containing dried electrolyte without the addition of NBH (see previous section). Additionally, the 0.1 M NBH electrolyte also shows an electron transfer number below one in ORR and OER in the fourth and sixth cycle. The reasons for this behavior, such as O_2 trapping and release in an interphase layer, can only be speculated upon.

The addition of borohydride shows a potential for improving the ORR/OER reversibility and for decreasing the rate of passivation. However, passivation is still pronounced and limits the improved reversibility to only a few cycles and short times. Most likely, this results from the lower amount of residual water in the electrolytes, which changes the composition of the surface layer formed on the electrode during the ORR, making it more oxidizable and, thus, suppressing the passivation of the electrode layer. However, we cannot rule out that NBH also acts as a complexing agent that could mask the Mg ions, similar to the crown ether. This is supported by the fact that 0.01 M NBH is sufficient to remove the residual water; therefore, there should be no major difference in the ORR/OER reaction behavior between the two NBH-containing electrolytes if it only acts as a water-removing additive. The ability of borohydrides to complex Mg ions has been reported.[49] Shao et al. have shown that the Mg plating and stripping behavior in different electrolyte strongly depends on the coordination of the electrochemically active Mg^{2+} species in the solution.[50] They reported enhanced Mg stripping when a combination of a chelating solvent and an increased BH_4^- concentration was used and explained this by synergetic effects.[50] Similar effects could be expected after the addition of NBH to $Mg(TFSI)_2$-containing electrolyte, in which NBH adopts both roles, that of the complexing agent and that of the water-removing agent.

Overall, the data indicate that a balance is required between minimizing the passivation (slow formation of the passivation layer at the electrode) and maximizing the reversibility (efficient formation of a layer of oxidizable ORR products on or close to the electrode surface). The lowest passivation was found for the 1 M crown-ether-containing electrolyte; however, the reversibility is rather limited (ORR/OER charge: 10:1). In contrast, the highest reversibility, with an ORR/OER charge of 1.7:1, was found in 0.1 M NBH-containing electrolyte; however, the passivation was much faster. Among the electrolytes investigated in this study, the 0.2 M crown-ether-containing electrolyte, with a Mg/crown ether ratio of 1:2, was the optimum choice, combining reasonable reversibility and limited passivation.

Finally, on a quantitative scale, the reversibility is expected to be different in a realistic battery cell as compared with the present flow cell measurements, as there would be no convection-induced off-transport of oxidizable ORR products. Additionally, compared with real batteries, the potential scan rate is much faster in the present measurements. Under realistic operation conditions, charging and discharging times would be longer than in the present experiments, resulting in much more extended accumulation of ORR products and electrolyte decomposition products before these are re-oxidized. This will be the subject of future studies.

Conclusions

The effect of adding crown ether as a typical complexing additive and borane dimethylamine complex (NBH) as an electrolyte drying additive to magnesium-containing *N*-butyl-*N*-methylpyrrolidinium bis(trifluoromethanesulfonyl)imide ([BMP][TFSI]) electrolytes was investigated to gain a better understanding of the influence of additives on the oxygen oxidation reaction (ORR)/oxygen evolution reaction (OER) in Mg–air batteries. The addition of a high stoichiometric excess of 18-crown-6 resulted in an increasingly effective masking of the Mg ions by complexation, which lowered the tendency for electrode passivation through the formation of nonoxidizable and passivating Mg (per-)oxides, to the extent observed in Mg-free [BMP][TFSI] electrolyte if 1.0 M 18-crown-6 ether is added to 0.1 M $Mg(TFSI)_2$. On the other hand, the complexation of Mg ions resulted in reduced formation/stabilization of re-oxidizable ORR products close to the electrode, which diminished the OER current/charge as the ORR products were rinsed away by the constant electrolyte flow. Under the present conditions, in a flow cell system, such an interphase layer is needed for a reversible ORR/OER even though it might result in some degree of passivation. Under the present reaction conditions and for the electrolytes investigated in this study, the best balance between passivation and reversibility was obtained for the 0.2 M crown-

ether-containing electrolyte with a Mg/crown ether ratio of 1:2.

The addition of NBH also resulted in a slower passivation and a better reversibility when it was added at a concentration of 0.1 M. This was most probably not only caused by its water-removing properties, but also by complexation of Mg^{2+}, similar to the role of the crown ether additive. Accordingly, if the concentration of NBH is too high, the reversibility of the ORR/OER is reduced. Overall, this work revealed a complex role of different additives, which should be considered in further efforts to improve the ORR/OER performance of Mg–air batteries.

Experimental Section

The electrochemical experiments were performed in a home-built DEMS setup (potentiostat: Pine Instruments, AFRDE 5; quadrupole mass spectrometer: Pfeiffer Vacuum, QMS 422), which has been described in detail by Schnaidt et al.[25] The key element of this set-up is a dual thin-layer flow cell equipped with a nonporous 10 μm thick Teflon membrane, which separates the electrolyte from the vacuum in the mass spectrometer chamber.

[BMP][TFSI] (99.9%, halides $\leq$ 1 ppm; $H_2O \leq 20$ ppm, Solvionic), $Mg(TFSI)_2$ (99.5%, $H_2O \leq 250$ ppm, Solvionic), 18-crown-6 (99.0%, $H_2O \leq 0.29$%, Alfa Aesar), and borane dimethylamine complex (NBH, 97%, Sigma–Aldrich) were used for the preparation of the electrolytes. They were mixed inside a glove box (MBraun, LabStar, Ar, $H_2O < 1$ ppm, $O_2 < 0.5$ ppm). After mixing the electrolytes we measured the water content through Karl Fischer titration for the pure BMP TFSI, the 0.1 M $MgTFSI_2$-containing BMP TFSI and the 0.1 M NBH-containing BMP TFSI, using a Mettler Toledo C30 coulometric KF titrator and a drying oven D0308 (Mettler Toledo). All electrolytes were transferred through air into a vacuum chamber, which was used for drying and storing the electrolytes. For drying of the NBH-free electrolytes prior to the DEMS measurements, they were evacuated at 10^{-7} mbar for $>$12 h. The NBH-containing electrolytes were not dried further owing to the instability of the NBH in vacuum. After drying, the electrolytes were purged with O_2 (MTI, N 6.0) and stored in a N_2 atmosphere in the same chamber used for electrolyte drying. However, the O_2 content of the electrolytes was not the same for all electrolytes because it was adjusted to not reach the faradaic current limitation of the electrochemical cell given by the low conductivity of the electrolyte. Therefore, a quantitative comparison of the absolute ORR current density values in the different measurements was not possible. For the electrochemical measurements, the electrolyte was pumped in a loop (total volume 10 mL) between the chamber and the flow cell by a peristaltic pump (Ismatek, Reglo ICC) at a flow rate of 0.13 mL min^{-1}. The capillary pumping system was surrounded by N_2-flushed tubes to reduce the amount of moisture and O_2 diffusing through the capillary walls.[22]

A glassy carbon (GC) disk (polished with a 0.3 μm alumina slurry prior to use) and a Pt wire (Goodfellow, 99.99+, diameter 0.5 mm) were used as working electrode and counter electrode, respectively. A Mg wire (Goodfellow, 99.99+, diameter 0.25 mm) with a native oxide film (Mg/MgO; −1.0 vs. Fc/Fc^+) served as a quasi-reference electrode.[23] The sensitivity factor k^* of the DEMS measurements was determined assuming a one electron transfer ($n = 1$) for the first reduction step ($E > -0.4$ V) of the ORR in neat [BMP][TFSI], using the ratio between the ion current of the m/z 32 signal (I_{32}) and the Faradaic current (I_F) according to the equation $k^* = nI_{MS}/I_F$.[22] The ion currents plotted in the figures were corrected for the background and for the time delay owing to mass transport of the gaseous species from the working electrode to and through the membrane.

The SEM and energy dispersive X-ray spectroscopy (EDX) measurements of the electrode layers were performed in a Zeiss Leo 1550 instrument, which was equipped with an Oxford Instruments EDX sensor. Before the SEM/EDX measurements, the electrode was rinsed with acetone (VWR chemicals, $\geq$99%) after removal from the flow cell and kept under an N_2 flow until it was introduced into the microscope.

Acknowledgements

This work was supported by the German Federal Ministry of Education and Research (BMBF) through projects 03X4636C and 03EK3051C and by the Deutsche Forschungsgemeinschaft through project Be 1201/22-1. The authors would also like to thank Cecilia Flores and Monja Schilling for their contribution to the DEMS measurements and Alexander Minkow of the Institute of Functional Nanosystems, Ulm University, for performing the SEM measurements. We would also like to thank Hanno M. Schütz (Helmholtz Institute Ulm) for performing the Karl-Fischer titration. This work contributes to the research performed at CELEST (Center for Electrochemical Energy Storage Ulm-Karlsruhe).

Conflict of interest

The authors declare no conflict of interest.

Keywords: differential electrochemical mass spectrometry · ionic liquids · magnesium · oxygen evolution reaction · oxygen reduction reaction

[1] A. R. Mainar, E. Iruin, L. C. Colmenares, A. Kvasha, I. de Meatza, M. Bengoechea, O. Leonet, I. Boyano, Z. Zhang, J. Alberto Blazquez, *J. Energy Storage* **2018**, *15*, 304–328.
[2] Y. Li, H. Dai, *Chem. Soc. Rev.* **2014**, *43*, 5257–5275.
[3] J. S. Lee, S. Tai Kim, R. Cao, N. S. Choi, M. Liu, K. T. Lee, J. Cho, *Adv. Energy Mater.* **2011**, *1*, 34–50.
[4] Z. Wang, D. Xu, J. J. Xu, X. B. Zhang, *Chem. Soc. Rev.* **2014**, *43*, 7746–7786.
[5] M. Xu, D. G. Ivey, Z. Xie, W. Qu, *J. Power Sources* **2015**, *283*, 358–371.
[6] J. Fu, Z. P. Cano, M. G. Park, A. Yu, M. Fowler, Z. Chen, *Adv. Mater.* **2017**, *29*, 1604685.
[7] P. Gu, M. Zheng, Q. Zhao, X. Xiao, H. Xue, H. Pang, *J. Mater. Chem. A* **2017**, *5*, 7651–7666.
[8] J. Fu, R. Liang, G. Liu, A. Yu, Z. Bai, L. Yang, Z. Chen, *Adv. Mater.* **2019**, *31*, 1805230.
[9] F. Mizuno, S. Nakanishi, Y. Kotani, S. Yokoishi, H. Iba, *Electrochemistry* **2010**, *78*, 403–405.
[10] M. A. Rahman, X. Wang, C. Wen, *J. Electrochem. Soc.* **2013**, *160*, A1759–A1771.
[11] T. Zhang, Z. Tao, J. Chen, *Mater. Horiz.* **2014**, *1*, 196–206.
[12] H. D. Yoo, I. Shterenberg, Y. Gofer, G. Gershinsky, N. Pour, D. Aurbach, *Energy Environ. Sci.* **2013**, *6*, 2265–2279.
[13] R. Mohtadi, F. Mizuno, *Beilstein J. Nanotechnol.* **2014**, *5*, 1291.
[14] Z. Ma, D. R. MacFarlane, M. Kar, *Batteries Supercaps* **2019**, *2*, 115–127.
[15] G. Vardar, J. G. Smith, T. Thompson, K. Inagaki, J. Naruse, H. Hiramatsu, A. E. S. Sleightholme, J. Sakamoto, D. J. Siegel, C. W. Monroe, *Chem. Mater.* **2016**, *28*, 7629–7637.
[16] D. Sharon, D. Hirshberg, M. Afri, A. A. Frimer, *J. Solid State Electrochem.* **2017**, *21*, 1861–1878.

[17] Y. Sun, X. Liu, Y. Jiang, J. Li, J. Ding, W. Hu, C. Zhong, *J. Mater. Chem. A* **2019**, *7*, 18183 – 18208.
[18] T. Kuboki, T. Okuyama, T. Ohsaki, N. Takami, *J. Power Sources* **2005**, *146*, 766 – 769.
[19] J. Zhang, A. M. Bond, *Analyst* **2005**, *130*, 1132 – 1147.
[20] M. Armand, J.-M. Tarascon, *Nature* **2008**, *451*, 652.
[21] M. Armand, F. Endres, D. R. MacFarlane, H. Ohno, B. Scrosati, *Nat. Mater.* **2009**, *8*, 621 – 629.
[22] G. Girishkumar, B. McCloskey, A. C. Luntz, S. Swanson, W. Wilcke, *J. Phys. Chem. Lett.* **2010**, *1*, 2193 – 2203.
[23] G. T. Cheek, W. E. O'Grady, S. Z. El Abedin, E. M. Moustafa, F. Endres, *J. Electrochem. Soc.* **2008**, *155*, D91 – D95.
[24] G. Vardar, A. E. S. Sleightholme, J. Naruse, H. Hiramatsu, D. J. Siegel, C. W. Monroe, *ACS Appl. Mater. Interfaces* **2014**, *6*, 18033 – 18039.
[25] J. Schnaidt, T. L. Nguyen, Z. Jusys, R. J. Behm, *Electrochim. Acta* **2019**, *299*, 372 – 377.
[26] M. Bozorgchenani, P. Fischer, J. Schnaidt, T. Diemant, R. M. Schwarz, M. Marinaro, M. Wachtler, L. Jörissen, R. J. Behm, *ChemElectroChem* **2018**, *5*, 2600 – 2611.
[27] Y. T. Law, J. Schnaidt, S. Brimaud, R. J. Behm, *J. Power Sources* **2016**, *333*, 173 – 183.
[28] Z. Jusys, J. Schnaidt, R. J. Behm, *J. Chem. Phys.* **2019**, *150*, 041724.
[29] D. Alwast, J. Schnaidt, K. Hancock, G. Yetis, R. J. Behm, *ChemElectroChem* **2019**, *6*, 3009 – 3019.
[30] Y. NuLi, J. Yang, J. Wang, J. Xu, P. Wang, *Electrochem. Solid-State Lett.* **2005**, *8*, C166.
[31] M. Kar, B. Winther-Jensen, M. Armand, T. J. Simons, O. Winther-Jensen, M. Forsyth, D. R. MacFarlane, *Electrochim. Acta* **2016**, *188*, 461 – 471.
[32] F. Sagane, K. Ogi, A. Konno, K. Kanamura, *J. Electrochem. Soc.* **2019**, *166*, A5054 – A5058.
[33] S. Matsuda, K. Uosaki, S. Nakanishi, *J. Power Sources* **2017**, *353*, 138.
[34] D. Alwast, J. Schnaidt, Z. Jusys, R. J. Behm, *J. Electrochem. Soc.* **2020**, *167*, 070505.
[35] F. Sagane, K. Ogi, A. Konno, M. Egashira, K. Kanamura, *Electrochemistry* **2016**, *84*, 76 – 78.
[36] Y. Katayama, H. Onodera, M. Yamagata, T. Miura, *J. Electrochem. Soc.* **2004**, *151*, A59 – A63.
[37] E. E. Switzer, R. Zeller, Q. Chen, K. Sieradzki, D. A. Buttry, C. Friesen, *J. Phys. Chem. C* **2013**, *117*, 8683 – 8690.
[38] X. Z. Yuan, V. Alzate, Z. Xie, D. G. Ivey, E. Dy, W. Qu, *J. Electrochem. Soc.* **2014**, *161*, A458 – A466.
[39] X. Z. Yuan, V. Alzate, Z. Xie, D. G. Ivey, W. Qu, *J. Electrochem. Soc.* **2014**, *161*, A451 – A457.
[40] J. Herranz, A. Garsuch, H. A. Gasteiger, *J. Phys. Chem. C* **2012**, *116*, 19084 – 19094.
[41] S. Monaco, A. M. Arangio, F. Soavi, M. Mastragostino, E. Paillard, S. Passerini, *Electrochim. Acta* **2012**, *83*, 94 – 104.
[42] A. W. Lodge, M. J. Lacey, M. Fitt, N. Garcia-Araez, J. R. Owen, *Electrochim. Acta* **2014**, *140*, 168 – 173.
[43] I. Weber, M. Eckardt, J. Schnaidt, R. J. Behm, unpublished results.
[44] N. N. Rajput, X. Qu, N. Sa, A. K. Burrell, K. A. Persson, *J. Am. Chem. Soc.* **2015**, *137*, 3411 – 3420.
[45] P. Reinsberg, C. Bondue, H. Baltruschat, *Electrochim. Acta* **2016**, *200*, 214 – 221.
[46] J. G. Smith, J. Naruse, H. Hiramatsu, D. J. Siegel, *Chem. Mater.* **2017**, *29*, 3152 – 3163.
[47] M. Mao, T. Gao, S. Hou, C. Wang, *Chem. Soc. Rev.* **2018**, *47*, 8804 – 8841.
[48] G. Vardar, E. G. Nelson, J. G. Smith, J. Naruse, H. Hiramatsu, B. M. Barlett, A. E. S. Sleightholme, D. J. Siegel, C. W. Monroe, *Chem. Mater.* **2015**, *27*, 7564 – 7568.
[49] M. Bremer, G. Linti, H. Nöth, M. Thomann-Albach, G. E. W. J. Wagner, *Z. Anorg. Allg. Chem.* **2005**, *631*, 683 – 697.
[50] Y. Shao, T. Liu, G. Li, M. Gu, Z. Nie, M. Engelhard, J. Xiao, D. Lv, C. Wang, J. G. Zhang, *Sci. Rep.* **2013**, *3*, 3130.

Manuscript received: March 14, 2020
Revised manuscript received: April 20, 2020
Accepted manuscript online: April 21, 2020
Version of record online: June 11, 2020

